

General analysis of the modulated-photocurrent experiment including the contributions of holes and electrons

C. Longeaud and J. P. Kleider

*Laboratoire de Génie Electrique de Paris, Ecole Supérieure d'Electricité, Université Paris VI,
Plateau de Moulon, 91192 Gif-sur-Yvette CEDEX, France*

(Received 13 November 1991)

In this paper we concentrate on an analysis of the modulated photocurrent (MPC) experiment applied to samples of amorphous semiconductors built in coplanar geometry. Taking into account both types of photocarriers, the basic equations describing the modulation of the occupation of the localized states are derived according to the statistics of Simmons and Taylor. Generalized expressions for the phase shift and the modulus of the modulated photocurrent are obtained without any restrictive assumptions and discussed. It is shown that, if one type of carrier is predominant, the modulated photocurrent gives the density as well as the capture cross section of the localized states interacting with these carriers. The precise conditions under which the two-carrier system is reduced to a single-carrier system are given. The main features of the method are illustrated by means of a simulation, where we study the influence of several parameters. We show that the dominant contribution to the modulated photocurrent comes from the carrier type which presents the higher value of $\mu/(N\sigma)$, where μ is the free-carrier mobility; σ , the capture cross section; and N , the density of trapping states for which the emission rate is equal to the angular frequency ω at which the experiment is performed. Consequently, only the trapping states corresponding to this type of carrier can be probed. Our study underlines some possible experimental misuses of the MPC technique which could lead to erroneous results regarding the inferred density of states.

I. INTRODUCTION

The knowledge of the density of states (DOS) in the gap of amorphous semiconductors is of great interest, since the localized states govern the transport properties in these materials. A wide variety of experiments has thus been devoted to that purpose.

Among these experiments, the photocurrent measurements, either of the transient or of the steady-state type, are good candidates. Indeed, the photocurrent reflects the free-carrier densities, which in turn depend on the DOS. Electrons undergo trapping and release processes with the states located essentially in the upper half of the gap (these states will be called electron states and the corresponding DOS will be called electron DOS in the following), while the holes interact essentially with the localized states located below midgap (these states will be called hole states and the corresponding DOS will be called hole DOS in the following). These two populations are coupled and equilibrate via recombination processes, which take place through the deepest gap states located around midgap. Due to these different interactions between free carriers and localized states, it is easily understood that the study of the photocurrent can lead to a determination of the DOS. However, the major problem in the analysis of the photocurrent is to evaluate both the electron and hole contributions and, if possible, to separate them in order to know which part of the DOS (electron or hole DOS) can effectively be probed. This can be done, for instance, by using specific experimental conditions such that the contribution of one type of car-

rier is predominant. An example is the time-of-flight technique performed on samples built on stacked geometry (for instance, Schottky diodes), where photocarriers are created locally by a short flash of light at one end of the sample and separated by the electric field coming either from an internal barrier or from the external applied voltage. Consequently, only one type of carrier drifts across the sample and the measured current is a signature of the trapping and release kinetics of these carriers. Thus, the analysis of the pretransit or posttransit photocurrents^{1,2} leads to the determination of the corresponding DOS.

Such a separation of both carrier contributions cannot be achieved easily in uniformly illuminated samples with coplanar electrodes that are often used to perform photocurrent measurements. In the modulated photocurrent (MPC) experiment, the semiconductor layer is illuminated with an excitation light which varies periodically with time. Due to the interactions with the localized states, there is a phase shift between the excitation and the alternative part of the resulting photocurrent. From an analysis based on the assumption of a unipolar photocarrier system, Oheda has shown how the study of this phase shift and its evolution with the excitation frequency could lead to a DOS spectroscopy,³ and he applied the technique to the study of the DOS in CdS crystals. The sensitivity of this technique was analyzed later by Aktas, Çil, and Aktulga,⁴ and Brüggemann, Main, Berkin, and Reynolds⁵ by means of numerical simulations. The latter authors have proposed an alternative treatment to the one proposed by Oheda for the determination of the DOS, us-

ing both the phase shift and the modulus of the modulated photocurrent (instead of only the phase shift, which required a recursive procedure) and have applied it to the determination of the DOS in As_2Se_3 . Meanwhile, this technique was applied to $a\text{-Si:H}$ by Schumm, Nitsch, and Bauer^{6,7} using the same treatment as Oheda.

It is noteworthy that the treatments proposed for the DOS spectroscopy give only *relative* DOS values. The determination of *absolute* DOS values requires the knowledge of the capture cross-section value since these two quantities always appear as a product. Besides, it is also required for a proper energy scaling of the DOS. The problem of energy scaling has been a matter of controversy in $a\text{-Si:H}$,⁸⁻¹⁰ and there is still a lack of direct experimental determination of the capture cross section in intrinsic amorphous semiconductors deposited in coplanar geometry. Moreover, all the above-mentioned authors used the same theoretical background as Oheda and did not take into consideration the possibility that Oheda's original analysis could be obscured by the contribution of both types of carriers to the photocurrent, at least when studying samples built in coplanar geometry.

In this paper we present an extension of the theoretical analysis of the MPC experiment, taking into account both types of photocarriers, and we focus on the problems indicated above. In particular, we show how the MPC can also be used to determine the capture cross section of gap states, thus allowing an *absolute* DOS spectroscopy. The reliability of the DOS shape inferred from the simple treatment based on the unipolar photocarrier system approach is also studied.

In Sec. II, the basic equations including the contributions of holes and electrons are presented and the generalized expressions of the phase shift and the modulus of the modulated photocurrent including both contributions are derived and discussed. Simplified expressions are then given in two main cases: for modulated photocurrents controlled by trapping and release processes or controlled by recombination processes.

In Sec. III, we show that, in the trapping- and release-limited regime, the generalized equations can be reduced to the simplified treatment giving the relative DOS spectroscopy as developed by previous workers if one assumes the contribution of one type of carriers to be predominant in the modulated photocurrent. We then show how the corresponding capture cross section of the gap states can be deduced from the transition between the recombination limited and the trapping- and release-limited regimes.

In Sec. IV, we present the results obtained from numerical calculations using our generalized equations. Transport and trapping parameters as well as an arbitrary DOS are introduced in the simulation and the continuous and modulated parts of the photocurrent due to a sinusoidal excitation are derived without any assumptions. The simplified treatment is then applied to the calculated phase shift and modulus in order to deduce a DOS shape, which is compared to the introduced DOS. The reliability of the deduced DOS is then studied as a function of different parameters, either intrinsic to the material (the shape of the DOS itself, the extended states

mobilities, the attempt-to-escape frequencies), or experimentally monitored (the photon flux intensity).

II. GENERALIZED ANALYSIS OF THE MODULATED PHOTOCURRENT

A. Basic equations

We consider a semiconductor layer in a coplanar configuration uniformly illuminated so that the concentrations of electrons and holes in the extended states (respectively, n and p) are uniform in the conduction cross section S . The general expression for the current I is then given by

$$I = Sq\xi(\mu_n n + \mu_p p), \quad (1)$$

where q is the absolute value of the electronic charge, ξ is the applied electric field, μ_n and μ_p are the extended-state mobilities of electrons and holes, respectively.

The values of n and p can be derived through the basic equations coming from the Shockley-Read statistics¹¹ in which it is assumed that traps can exchange electrons and holes via the conduction and valence band, respectively. Simmons and Taylor¹² have extended this statistics to an arbitrary distribution of traps. With the electron and hole current densities being uniform, the continuity equations for electrons and holes are

$$\frac{\partial n}{\partial t} = G - \int_{E_v}^{E_c} \bar{n} N(E) [1 - f(E)] dE + \int_{E_v}^{E_c} e_n(E) N(E) f(E) dE, \quad (2)$$

$$\frac{\partial p}{\partial t} = G - \int_{E_v}^{E_c} \bar{p} N(E) f(E) dE + \int_{E_v}^{E_c} e_p(E) N(E) [1 - f(E)] dE, \quad (3)$$

where t is the time, $N(E)$ is the DOS at the energy E , $f(E)$ is the probability of a state at the energy E to be occupied by an electron (called the occupation function in the following), G is the generation rate of carriers, $e_n(E)$ and $e_p(E)$ are the emission rates of electrons and holes from a state at the energy E toward the conduction and valence band, respectively; \bar{n} and \bar{p} are the capture rates of electrons and holes which can be written $\bar{n} = v_n \sigma_n n = c_n n$ and $\bar{p} = v_p \sigma_p p = c_p p$, v_n and v_p being the thermal velocities, σ_n and σ_p the capture cross sections, and c_n and c_p the corresponding capture coefficients for electrons and holes, respectively. In the following we shall consider only a single species of traps, so that σ_n and σ_p are assumed to be independent of the energy. According to the Shockley-Read statistics, the occupation function $f(E)$ is given by

$$\frac{\partial f(E)}{\partial t} = \bar{n} + e_p(E) - f(E) [\bar{n} + \bar{p} + e_n(E) + e_p(E)]. \quad (4)$$

Since in the MPC experiment the excitation light is a periodic function of the time, two types of contributions have to be considered: the first one giving rise to a dc current due to the average contribution of the excitation to the creation of carriers and the second one coming

from the alternative part of the excitation. We treat the case of a small ac signal and do not take the harmonics into consideration. So, basically all the quantities appearing in Eqs. (2) and (3), except the emission rates and $N(E)$, can be separated in two components indexed dc for the steady-state component and ac for the alternative component. For instance, n is replaced by $n = n_{dc} + n_{ac} \exp(j\omega t)$ where j is the purely imaginary number such that $j^2 = -1$ and ω is the pulsation of the excitation. Since we expect a phase shift between the excitation and the resulting current, n_{ac} is a complex quantity. Taking into account both the dc and ac components, Eqs. (2) and (3) lead to

$$0 = G_{dc} - \int_{E_v}^{E_c} \bar{n}_{dc} N(E) [1 - f_{dc}(E)] dE + \int_{E_v}^{E_c} e_n(E) N(E) f_{dc}(E) dE, \quad (5)$$

$$0 = G_{dc} - \int_{E_v}^{E_c} \bar{p}_{dc} N(E) f_{dc}(E) dE + \int_{E_v}^{E_c} e_p(E) N(E) [1 - f_{dc}(E)] dE, \quad (6)$$

for the steady-state contribution and to

$$j\omega n_{ac} = G_{ac} + \int_{E_v}^{E_c} \{[\bar{n}_{dc} + e_n(E)] f_{ac}(E) - \bar{n}_{ac} [1 - f_{dc}(E)]\} N(E) dE, \quad (7)$$

$$j\omega p_{ac} = G_{ac} - \int_{E_v}^{E_c} \{[\bar{p}_{dc} + e_p(E)] f_{ac}(E) + \bar{p}_{ac} f_{dc}(E)\} N(E) dE, \quad (8)$$

for the alternative contribution. In the same way, Eq. (4) gives

$$f_{dc}(E) = \frac{\bar{n}_{dc} + e_p(E)}{\bar{n}_{dc} + \bar{p}_{dc} + e_n(E) + e_p(E)} \quad (9)$$

and

$$f_{ac}(E) = \frac{\bar{n}_{ac} [1 - f_{dc}(E)] - \bar{p}_{ac} f_{dc}(E)}{j\omega + 1/\tau}, \quad (10)$$

where

$$\frac{1}{\tau} = \bar{n}_{dc} + \bar{p}_{dc} + e_n(E) + e_p(E). \quad (11)$$

In these equations, $\bar{n}_{dc} = c_n n_{dc}$, $\bar{p}_{dc} = c_p p_{dc}$, $\bar{n}_{ac} = c_n n_{ac}$, and $\bar{p}_{ac} = c_p p_{ac}$.

For a given DOS, given capture cross sections and free-carrier mobilities, the ac component of the photocurrent can be calculated if we know n_{ac} and p_{ac} . These are obtained from Eqs. (7) and (8). However, note that the resolution of Eqs. (7) and (8) is possible only if the values of n_{dc} , p_{dc} , as well as the energy variations of f_{dc} have been calculated from Eqs. (5), (6), and (9), taking into account the charge neutrality. In the case of amorphous semiconductors, for which the excess free carriers are orders of magnitude less numerous than the trapped carriers, and assuming that the capture cross sections are independent of the energy, the statement of charge neutrality can be written¹³

$$\bar{n}_{dc} \int_{E_F}^{E_{tn}} N(E) dE = \bar{p}_{dc} \int_{E_{tp}}^{E_F} N(E) dE, \quad (12)$$

where E_F is the equilibrium Fermi level and E_{tn} and E_{tp} are the quasi-Fermi-levels for trapped electrons and trapped holes, respectively. The calculation of n_{dc} , p_{dc} , and $f_{dc}(E)$ has been extensively treated by Simmons and Taylor.¹⁴ In the following we shall derive the expression of the modulated photocurrent from the resolution of Eqs. (7) and (8).

B. Expressions of the phase shift and modulus of the modulated photocurrent

If the expression of $f_{ac}(E)$ given by Eq. (10) is replaced in Eqs. (7) and (8) and writing $n_{ac} = n_r + jn_i$, $p_{ac} = p_r + jp_i$, the indexes r and i standing for real and imaginary, respectively; a linear system of four equations is obtained:

$$\begin{aligned} A_n n_i + A_p p_i + B_n n_r - B_p p_r &= 0, \\ B_n n_i - B_p p_i - A_n n_r - A_p p_r &= -G_{ac}, \\ A_n^* n_i + A_p^* p_i - B_n^* n_r + B_p^* p_r &= 0, \\ -B_n^* n_i + B_p^* p_i - A_n^* n_r - A_p^* p_r &= -G_{ac}, \end{aligned} \quad (13)$$

where the expressions of A_n , B_n , A_p , B_p , A_n^* , B_n^* , A_p^* , and B_p^* are given in the Appendix. If the linear system given by Eq. (13) is solved for n_r , n_i , p_r , and p_i , the alternative contribution to the photocurrent is found from

$$I_{ac} = Sq \xi [\mu_n n_r + \mu_p p_r + j(\mu_n n_i + \mu_p p_i)]. \quad (14)$$

Then, the phase shift Φ between the excitation and the modulated photocurrent as well as the modulus of this photocurrent such as $I_{ac} = |I_{ac}| \exp(-j\Phi)$ are given by

$$\tan(\Phi) = -\frac{\mu_n n_i + \mu_p p_i}{\mu_n n_r + \mu_p p_r}, \quad (15)$$

$$|I_{ac}| = Sq \xi [(\mu_n n_i + \mu_p p_i)^2 + (\mu_n n_r + \mu_p p_r)^2]^{1/2}. \quad (16)$$

The coefficients A_n , B_n , A_p , B_p , A_n^* , B_n^* , A_p^* , and B_p^* and consequently Φ and $|I_{ac}|$ can be numerically calculated with a microcomputer for a given DOS, given capture cross sections and mobilities of electrons and holes in the extended states.

Considering the physics involved, it is easily understood that two specific energy levels $E_{\omega n}$ and $E_{\omega p}$ such that

$$e_n(E_{\omega n}) = e_p(E_{\omega p}) = \omega, \quad (17)$$

play an important role. Depending on the relative position of these levels compared with the quasi-Fermi-levels for trapped carriers E_{tn} and E_{tp} , the energy limits of the recombination centers defined by $e_n(E_{tn}) = e_p(E_{tp}) = \bar{n}_{dc} + \bar{p}_{dc}$, two cases have to be considered: (i) $\omega \gg \bar{n}_{dc} + \bar{p}_{dc}$, where the modulated photocurrent is controlled by trapping and release processes, (ii) $\omega \ll \bar{n}_{dc} + \bar{p}_{dc}$, where the modulated photocurrent is controlled by recombination processes.

C. Simplified expressions in case (i) ($\omega \gg \bar{n}_{dc} + \bar{p}_{dc}$)

We have indicated in the Appendix that, because of the shape of $f_{dc}(E)$, some of the coefficients in Eq. (13) are negligible compared to the others. Actually, the dominant coefficients are A_n , B_n , A_p^* , and B_p^* and the linear system of four equations (13) then simply splits into two linear systems of two equations:

$$\begin{aligned} A_n n_i + B_n n_r &= 0, \\ B_n n_i - A_n n_r &= -G_{ac}, \end{aligned} \quad (18)$$

and

$$\begin{aligned} A_p^* p_i + B_p^* p_r &= 0, \\ B_p^* p_i - A_p^* p_r &= -G_{ac}. \end{aligned} \quad (19)$$

Equations (18) and (19) show that, as far as the alternative contribution is concerned, the populations of electrons and holes are no longer coupled and can be found separately from the resolution of the two subsystems (18) and (19). This is simply because the excess carrier populations in trapping states are in contact only with their nearest respective band. If we define the two quantities N_n and D_n by

$$N_n = \frac{B_n \mu_n}{A_n^2 + B_n^2}, \quad (20)$$

$$D_n = \frac{A_n \mu_n}{A_n^2 + B_n^2}, \quad (21)$$

and the two equivalent quantities N_p and D_p by the same relations using A_p^* , B_p^* , and μ_p instead of A_n , B_n , and μ_n , respectively, then the phase shift and the modulus of the photocurrent are obtained from

$$\tan(\Phi) = \frac{N_n + N_p}{D_n + D_p}, \quad (22)$$

and

$$|I_{ac}| = G_{ac} S q \xi \sqrt{(N_n + N_p)^2 + (D_n + D_p)^2}. \quad (23)$$

These are generalized expressions for $\tan(\Phi)$ and $|I_{ac}|$ including the contributions of both types of carriers.

D. Simplified expressions in case (ii) ($\omega \ll \bar{n}_{dc} + \bar{p}_{dc}$)

The system given by Eq. (13) cannot be splitted into two subsystems holding for each type of carrier separately. However, from calculations summarized in the Appendix, we reach the simple first-order approximate expressions:

$$\phi = 0, \quad (24)$$

and

$$|I_{ac}| = S q \xi G_{ac} (\mu_n \tau_n + \mu_p \tau_p). \quad (25)$$

This shows that, if the frequency is low enough, the ac photocurrent is no longer related to trapping and release processes, but is recombination limited and its expression is similar to the dc one.

III. DETERMINATION OF THE DENSITY AND CAPTURE CROSS SECTION OF THE LOCALIZED STATES

From the above results, we can calculate the modulated photocurrent if the DOS, capture cross sections, and mobilities in the extended states are given. In practice, the problem is to determine the gap states features from the measured modulated photocurrent. We show here that, if there is one dominant type of carriers, it is possible to deduce not only a *relative* DOS spectrum, as already pointed out by various authors,^{3,5} but also *absolute* DOS values as well as the capture cross section of the gap states.

A. Case (i) ($\omega \gg \bar{n}_{dc} + \bar{p}_{dc}$)

It is straightforward that, if the following inequalities are satisfied,

$$N_n \gg N_p, \quad (26a)$$

$$D_n \gg D_p, \quad (26b)$$

our generalized expressions (22) and (23) lead to the simpler ones corresponding to an electron controlled behavior:

$$\tan(\Phi) \approx \frac{B_n}{A_n}, \quad (27)$$

and

$$|I_{ac}| \approx \frac{G_{ac} S q \xi \mu_n}{\sqrt{A_n^2 + B_n^2}}, \quad (28)$$

which correspond to the expressions derived by Oheda.³

As shown by Brüggemann *et al.*,⁵ with the simplified expressions of A_n and B_n (see the Appendix), these equations lead to

$$\tilde{N}(E_{\omega n}) = \frac{2}{\pi \nu_n} \left[\frac{S q \mu_n \xi G_{ac} \sin(\Phi)}{|I_{ac}|} - \omega \right], \quad (29)$$

where $E_{\omega n}$ is defined according to Eq. (17) by

$$E_c - E_{\omega n} = k_B T \ln \left[\frac{\nu_n}{\omega} \right]. \quad (30)$$

$\tilde{N}(E_{\omega n})$ is the ratio of the DOS at $E_{\omega n}$ to the DOS at E_c , $\tilde{N}(E_{\omega n}) = N(E_{\omega n})/N(E_c)$, and ν_n the attempt-to-escape frequency defined by $\nu_n = c_n k_B T N(E_c)$, where k_B is the Boltzmann constant and T the temperature. An alternative method which uses the frequency dependence of the ratio $\cos(\phi)/|I_{ac}|$ has been recently suggested:¹⁵

$$\frac{\nu_n \tilde{N}(E_{\omega n})}{\mu_n} = S q \xi G_{ac} \omega \frac{d}{d\omega} \left[\frac{\cos(\Phi)}{|I_{ac}|} \right]. \quad (31)$$

In a similar way, if N_n , N_p , D_n , and D_p satisfy the opposite inequalities, that is if $N_p \gg N_n$ and $D_p \gg D_n$, then our general relations lead to the simpler ones corresponding to a hole controlled response. The relations for the phase shift and the modulus are then similar to Eqs. (27)

and (28) with A_p^* and B_p^* instead of A_n and B_n , and a relative DOS spectrum corresponding to hole states can be deduced in a similar way from Eqs. (29) and (30) or (30) and (31) using the subscript p instead of n , the energy scale being given by $E_{\omega p} - E_v$ instead of $E_c - E_{\omega n}$. The following features have to be emphasized.

(a) The proposed method is valid for both types of carriers if the angular frequency ω is greater than $\bar{n}_{dc} + \bar{p}_{dc}$. Only the localized states acting as trapping states (as opposed to recombination states) can then be probed. As a consequence, if we define the level E_F^* by $e_n(E_F^*) = e_p(E_F)$ if the material is p type or $e_n(E_F) = e_p(E_F^*)$ if the material is n type, the range of energy between the dark Fermi level E_F and E_F^* , which is roughly symmetrical to E_F with respect to midgap, is never available. This result is specific to a coplanar geometry with a uniform illumination; in a sandwich configuration, for instance, in a Schottky structure, this analysis does not apply, and one would have to study the free carrier concentration profiles in order to evaluate the recombination kinetics.

(b) Since the second term (ω) contained within the large parentheses of Eq. (29) is generally negligible, the information given from either Eq. (29) or Eq. (31) essentially concerns the value of $v\bar{N}(E_\omega)/\mu$ that is $v\sigma N(E_\omega)/\mu$, $v\sigma$ being the capture coefficient of the gap states interacting with the dominant carrier. As the value of v or σ is generally not well known, this means that only a *relative* DOS spectrum can be inferred, the *absolute* value of the DOS remaining unknown. Furthermore, the bad knowledge of the attempt-to-escape frequency can also lead to a distortion of the spectrum, because of an error in the energy scale [Eq. (30)].

(c) If neither the inequalities defined by Eq. (26), nor their opposites are satisfied, the contribution of electrons and holes to the modulated photocurrent cannot be separated and it is not possible to determine any part of the relative DOS shape in such a simple way. Thus, it appears important to determine the conditions on the transport and trapping parameters (free-carrier mobilities, DOS, and attempt-to-escape frequencies) so that the inequalities (26a) and (26b) are satisfied. This determination is not straightforward, even if one considers the simplified expressions of A_n , B_n , A_p^* , and B_p^* [Eqs. (A11), (A17), (A13), and (A18), respectively]. However, it can be observed that A_n and B_n are increasing functions of v_n and of the electron DOS, so that N_n and D_n are decreasing functions of v_n and of the electron DOS while they are proportional to the electron mobility. The same kind of dependences on the corresponding hole parameters can be set forth for A_p^* , B_p^* , N_p , and D_p . As a consequence, it is suggested that, if the DOS shape exhibits smooth variations, the modulated photocurrent will be controlled by the carriers for which the product $v\bar{N}(E_\omega)/\mu$ or $v\sigma N(E_\omega)/\mu$ is the smallest. This will be illustrated in Sec. IV.

B. Transition from case (i) to case (ii)

From the simplified expressions of the phase shift and modulus of the modulated photocurrent obtained in cases

(i) and (ii), it can be seen that the ratio $\cos(\phi)/|I_{ac}|$ is constant in case (i), while it is increasing with frequency in case (ii). Consequently, the angular frequency ω_0 corresponding to the transition between the two regimes, defined by

$$\omega_0 = \bar{n}_{dc} + \bar{p}_{dc}, \quad (32)$$

can be found experimentally. If the capture rate of one type of carriers is predominant, and if the same type of carriers has a major contribution to the total dc current, then it is possible to determine the corresponding capture cross section from a measurement of the threshold frequency. Suppose, for instance, that the electrons are the predominant type of carriers so that $\bar{p}_{dc} \ll \bar{n}_{dc}$ and $\mu_p p_{dc} \ll \mu_n n_{dc}$, then the value of n_{dc} is simply obtained from the measurement of the total dc current:¹⁶

$$n_{dc} = \frac{I_{dc}}{Sq\xi\mu_n} \quad (33)$$

so that the ratio of the capture coefficient to the mobility is deduced from

$$\frac{v_n\sigma_n}{\mu_n} = \frac{Sq\xi\omega_0}{I_{dc}}. \quad (34)$$

Even in the worst cases in which values of the electron mobility and thermal velocities are unknown, this can be used to obtain the *absolute* estimate of the DOS from Eq. (31). Fortunately, these values are in most cases well estimated from the theory or from other types of experiments, thus allowing the determination of the capture cross section, which can then be used for a proper energy scaling of the DOS.

IV. ILLUSTRATION BY MEANS OF A SIMULATION

A. Description of the simulation

Though our simulation [which is rather a numerical calculation of the coefficients of Eq. (13)] could be used to describe the behavior of any amorphous semiconductors exhibiting a density of localized states between the extended states, we have decided to focus on the case of a -Si:H.

We present in Fig. 1 the DOS which has been widely used in our simulations. This DOS has been chosen such as to be a representative of a -Si:H with a band gap width equal to 1.8 eV and the dark Fermi level E_F located at 0.75 eV below the conduction-band edge. This DOS can be divided into band tails and deep states. The shape of the band tails comes from experimental results obtained from the time-of-flight technique performed on standard a -Si:H and presented elsewhere.¹⁷ The shape of the deep states is suggested by the results of post-transit measurements² for the upper half of the gap, and by results obtained by photoyield spectroscopy¹⁸ for the lower half of the gap. This shape has been reproduced by means of two Gaussian functions. The values of the characteristic width and of the maximum are, respectively, $\sigma_1 = 0.24$ eV and $N_1 = 1.2 \times 10^{16} \text{ cm}^{-3} \text{ eV}^{-1}$ for the first Gaussian function which is centered at 0.55 eV below the

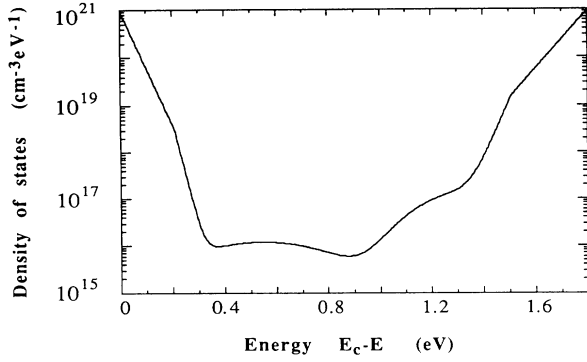


FIG. 1. Typical DOS introduced in our simulation. The shape of the DOS is representative of *a*-Si:H and suggested by different experimental results.

conduction-band edge E_c . The values of these parameters for the second Gaussian function centered at 1.3 eV below E_c are, respectively, $\sigma_2=0.14$ eV and $N_2=1.2\times 10^{17}$ cm $^{-3}$ eV $^{-1}$. With such a shape for the deep states, the value of the DOS at the dark Fermi level is $N(E_F)=8\times 10^{15}$ cm $^{-3}$ eV $^{-1}$ and the integral of the DOS between E_F and midgap is equal to 1×10^{15} cm $^{-3}$, two values which are in agreement with those found from capacitance measurements performed on standard *a*-Si:H.¹⁹ As seen in Fig. 1 we have chosen to take the same values for the DOS at the band edges: $N(E_c)=N(E_v)=10^{21}$ cm $^{-3}$ eV $^{-1}$.

The simulation runs in the following way: for a given dc generation rate G_{dc} , Eqs. (5), (6), and (12) are first solved in order to determine the free-carrier densities n_{dc} and p_{dc} , the variations of $f_{dc}(E)$ and the position of the quasi-Fermi-levels for trapped carriers E_{tn} and E_{tp} . The integrals are calculated by dividing the gap into 4500 steps each being 0.4 meV wide. Then the system (13) is solved for a given frequency at a given temperature and the values of the phase shift and of the modulus of the modulated photocurrent are calculated according to our generalized relations (15) and (16), respectively, the process being repeated for another frequency and/or another temperature.

We present in Fig. 2 typical results for the phase shift [Fig. 2(a)] and the modulus [Fig. 2(b)] of the modulated photocurrent obtained with the DOS presented in Fig. 1. The extended state mobilities μ_n and μ_p were taken equal to 10 cm $^{-2}$ V $^{-1}$ s $^{-1}$, and the attempt-to-escape frequencies ν_n and ν_p equal to 10 12 s $^{-1}$ (corresponding to values of the capture cross section of 4×10^{-15} cm 2 at 300 K). Each set of symbols shown in these figures, as well as in Figs. 4–7, is the result of the calculations obtained at a fixed temperature for a set of 21 frequencies varying from $f_1=12$ Hz to $f_{21}=39.9$ kHz (such as $f_{i+1}=1.5\times f_i$) as it could be achieved experimentally with a low cost standard light emitting diode. The temperature was varied in 25-K steps, but for clarity, we present in Figs. 2(a) and 2(b) only seven curves labeled according to the seven corresponding temperatures ranging from 150 K (curve labeled 1) to 450 K (curve labeled 7) in 50-K steps. The

limits of the temperature range have been chosen to fit the standard behaviors of *a*-Si:H. Indeed, 150 K represents the lower limit above which one can assume that direct transitions from one localized state to another can be neglected, whereas 450 K represents the upper limit above which some evolution of the material can occur. Experimentally, this upper limit must be lower than the deposition temperature of the *a*-Si:H layer. No direct relation between the phase shift or the modulus and the density of states is discernible on these figures, and one has to use one of the treatments exposed in Sec. III to interpret the data. From each set of coupled phase shift and modulus results corresponding to a given temperature, part of the DOS shape can then be deduced by means of Eqs. (29) and (30), and compared with the introduced DOS. We decided to use Eq. (29) instead of Eq. (31) for its simplicity and also because it does not involve any derivative. Even if one only uses temperatures varying in 50-K steps, there is an overlap from one temperature to the next one in the energy ranges explored by varying the frequency, and the corresponding parts of the deduced DOS shapes should overlap.

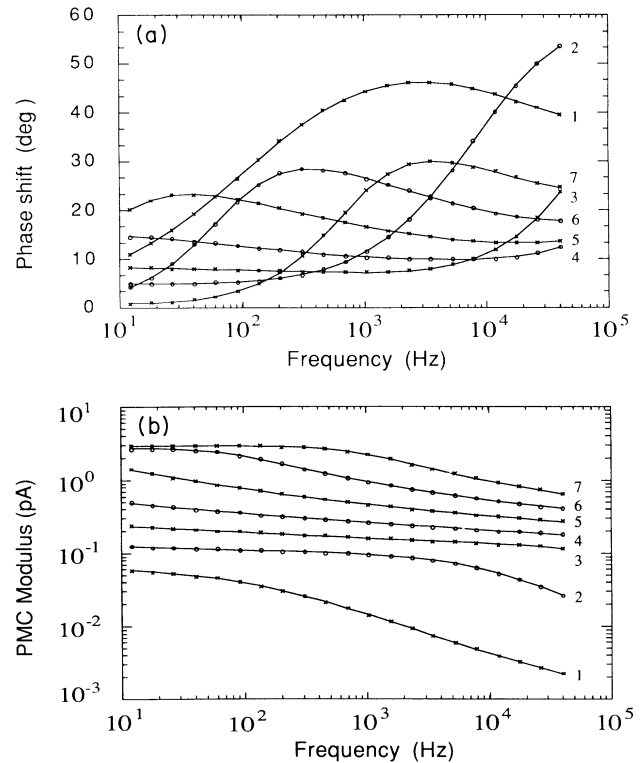


FIG. 2. (a) Typical variations of the phase shift and (b) of the modulus of the modulated photocurrent calculated from the simulation using the DOS of Fig. 1, and the following values for the geometrical and electrical parameters: $S=2.25\times 10^{-5}$ cm 2 , $\xi=3000$ V cm $^{-1}$, $\mu_n=\mu_p=10$ cm 2 V $^{-1}$ cm $^{-1}$, $\nu_n=\nu_p=10^{12}$ s $^{-1}$, $G_{dc}=2.4\times 10^{15}$ cm $^{-3}$ s $^{-1}$, and $G_{ac}=G_{dc}/10$. The frequency of the modulation was varied from 12 Hz to 39.9 kHz at a given temperature and the temperature varied from 150 K (curve labeled 1) to 450 K (curve labeled 7) in 50-K steps.

We have shown in Sec. II that, depending on the characteristics of the material (DOS shape, attempt-to-escape frequency, and mobility values), the modulated photocurrent can be representative either of the electron or of the hole trapping states. This is why, when comparing the DOS reconstructed from the simulation with the introduced DOS (Figs. 4–7), the energies have been referred either to the conduction-band edge E_c (corresponding then to the DOS above midgap) or to the valence-band edge E_v (corresponding then to the DOS below midgap). With this procedure, one can see immediately if the deduced DOS corresponds to the electron or to the hole states.

B. Influence of the photon flux

The carrier generation G_{dc} , giving rise to the dc current contribution, is a parameter one experimentally adjusts by varying the average contribution of the photon flux. It is physically of great interest since it determines the range of energy of the recombination centers. Consequently, it also determines, for given frequency and temperature, if the modulated photocurrent is controlled by trapping and release or by recombination processes. We present in Fig. 3(a) the plots of $\cos(\phi)/|I_{ac}|$ versus frequency obtained at $T=300$ K for five values of the dc photon flux ranging from $F/100$ to $F \times 100$, with $F=6 \times 10^{12} \text{ cm}^{-2} \text{ s}^{-1}$ (corresponding roughly to a dc gen-

eration rate equal to $G_{dc}=2.4 \times 10^{17} \text{ cm}^{-3} \text{ s}^{-1}$ if we take the absorption coefficient α equal to $4 \times 10^4 \text{ cm}^{-1}$). As expected from our analysis and the simplified analytical expressions given in Sec. II, $\cos(\phi)/|I_{ac}|$ is never constant for the lowest values of the dc flux ($F/10$ and $F/100$) for in the “measurement” frequency window, ω is always greater than $\bar{n}_{dc} + \bar{p}_{dc}$. As the dc flux is increased $\cos(\phi)/|I_{ac}|$ appears to be constant for the lower values of the frequency, and the extent in frequency of the constant part of the curves increases with the dc photon flux. These behaviors can be explained easily by the results obtained for $\omega \ll \bar{n}_{dc} + \bar{p}_{dc}$ and by the fact that n_{dc} and p_{dc} increase with the dc flux. At sufficiently high frequencies we have $\omega \gg \bar{n}_{dc} + \bar{p}_{dc}$ and the curves have the same dependence with ω , which is then linked to the DOS shape via Eq. (29). For very high dc flux ($F \times 100$) this regime is never reached since the frequency is always too low. We have indicated by an arrow the position of the turn-on frequency for which $\omega = \omega_0 = \bar{n}_{dc} + \bar{p}_{dc} = e_n(E_{in})$. One can see that it corresponds to the end of the constant regime.

We present in Fig. 3(b) the same curves obtained at $T=400$ K. Again the same trends can be observed. For all the values of the dc flux $\cos(\phi)/|I_{ac}|$ is first constant and then increases toward identical values for all the curves. In opposition to the behaviors observed in Fig. 3(a), a constant value of $\cos(\phi)/|I_{ac}|$ is obtained even at very low dc flux ($F/100$). This is because at this high temperature, the “probed” level E_ω always falls in the energy range of the recombination centers at low frequencies.

The curves of Fig. 3 show that the transition between the two regimes (i) and (ii) can be clearly identified, so that the capture cross section can be deduced with good accuracy on the basis of the above analysis. The value of the capture cross section can then be used to obtain the absolute magnitude of the DOS and a proper energy scaling from the regime (i) ($\omega \gg \bar{n}_{dc} + \bar{p}_{dc}$), which is also identified from these curves.

We present in Fig. 4, with various sets of symbols, the DOS shapes obtained from Eq. (29) under a photon flux $F/100$ [Fig. 4(a)] and F [Fig. 4(b)], the first results being deduced from the curves presented in Figs. 2(a) and 2(b). Clearly, the deduced DOS corresponds to *electron* trapping states. The agreement between the DOS deduced from Eq. (29) and the introduced DOS is quite good in Fig. 4(a) except for the three lowest temperatures (150, 200, and 250 K) when entering the conduction-band tail, where the corresponding sets of symbols can be well distinguished from one another. In this region, though the general trend is satisfactorily reproduced, the deduced DOS is always above the introduced one, and the variations are somewhat smooth. This can be explained in the light of the approximation made to derive the expression (29) in order to allow the simple DOS reconstruction, namely the Dirac function approximation of the weighting function $G_n(E)$ (see the Appendix). Indeed, if the DOS varies more rapidly than $\exp[|E|/(k_B T)]$, the Dirac function approximation attributes to the only level $E_{\omega n}$ a part of the signal originating from surrounding energies.

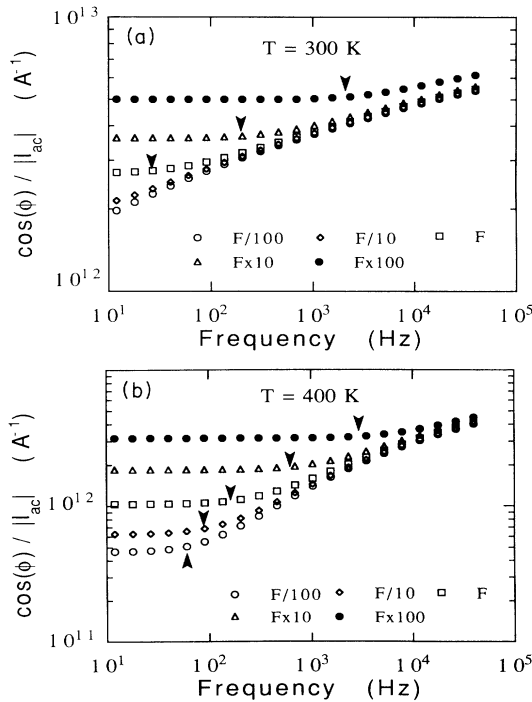


FIG. 3. Plots of $\cos(\phi)/|I_{ac}|$ vs frequency for five different values of the dc photon flux, (a) at $T=300$ K and (b) $T=400$ K. The threshold frequency corresponding to the transition between the trapping- and release-limited and the recombination-limited regime is indicated on each curve by an arrow.

This leads to an overestimation of $N(E_{\omega_n})$ and to a smoothing of the DOS, as it happens in the bottom of the conduction-band tail, which has very sharp variations in the considered energy range (the characteristic tempera-

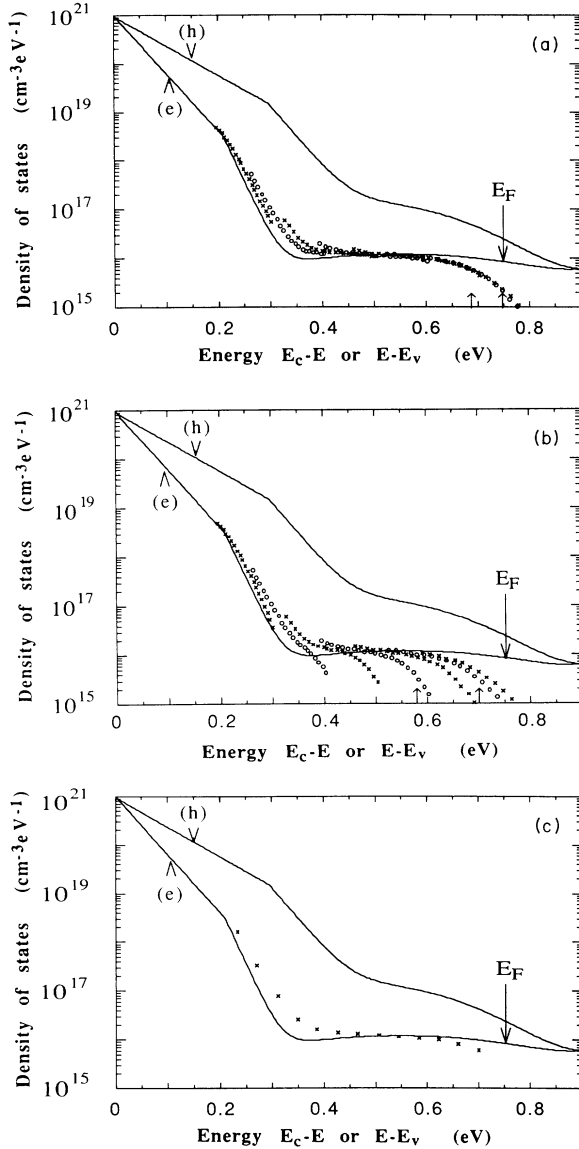


FIG. 4. The DOS calculated from the MPC phase shift and modulus (symbols) is compared with the actual DOS (full lines). The position of the dark Fermi level $E_c - E_F = 0.75$ eV is indicated by an arrow in all the figures. The labels (e) and (h) indicate the electron and hole DOS, that is the DOS on the conduction- and valence-band side, respectively. The generation due to the continuous part of the excitation light is equal to $G_{dc} = 2.4 \times 10^{15}$ cm $^{-3}$ s $^{-1}$ in (a) and $G_{dc} = 2.4 \times 10^{17}$ cm $^{-2}$ s $^{-1}$ in (b). The threshold frequencies at $T = 300$ and 400 K are indicated by arrows. In (c) the symbols represent the results one can obtain at 3.5 kHz by varying the temperature from 150 to 450 K in 25 -K steps, which are the same for both values of the dc generation rate. For all these figures, one can see that the deduced DOS shape is only representative of the *electron* trapping states.

ture of the slope of this exponential part is equal to 220 K). Another example of the influence of the shape of $G_n(E)$ has been given by Brüggemann *et al.*⁵ Indeed, these authors have shown how three discrete levels of traps transform into three large bumps, the shapes of which actually correspond to that of $G_n(E)$. We can say that a discrete level of traps is closer to a Dirac function than $G_n(E)$ so that the deduced DOS shape actually becomes that of $G_n(E)$ in this extreme case. Therefore care has to be taken if one observes experimentally rapid variations in the DOS, for the actual variations may be even sharper.

We further observe an increasing discrepancy between introduced and calculated DOS in the range of energy around the Fermi level E_F , for temperatures greater than 400 K, where the calculated DOS values exhibit a sharp drop and are systematically lower than the real ones. This is an artifact inherent to the method: when the probed energy E_{ω} approaches or falls in the energy range of the recombination centers, we know from the analysis performed in Sec. III that the modulated photocurrent is controlled by recombination and a DOS spectroscopy is no longer possible. As the modulus $|I_{ac}|$ of the photocurrent tends to be constant for decreasing frequencies, while the phase shift tends towards zero, any attempt to use the data in this range in order to derive a DOS shape by means of Eq. (29) leads to an artificial decreasing DOS for increasing $E_c - E$ values. Such a feature is expected to take place even well above the dark Fermi level if the dc photon flux is increased. This is indeed observed in Fig. 4(b) where the results are obtained under a photon flux equal to F . We have indicated on both figures the point corresponding to the turn-on frequency ω_0 at $T = 300$ and 400 K, deduced from Figs. 3(a) and 3(b). The deduced DOS at the threshold frequency is about five times smaller than the actual one, and one has to only use frequencies such as $\omega > 10\omega_0$ in order to keep the relative error within 50% . For these higher frequencies, the modulated photocurrent is well limited by trapping and release processes, and the DOS values calculated from Eq. (29) are independent on the value of the dc flux, as it can be seen from the comparison of the results presented on Figs. 4(a) and 4(b).

The preceding results indicate that one has to be careful when trying to probe the DOS of an amorphous semiconductor. In a first step, a frequency scan at each selected temperature and a plot of $\cos(\phi)/|I_{ac}|$ versus frequency as in Fig. 3 have to be performed in order to determine the value of the capture cross section which is necessary for an absolute scaling of the DOS and to figure out the frequency domain ($\omega > 10\omega_0$) from which the DOS can be probed by means of Eq. (29). Note that it is not possible to fix a universal value for the turn-on frequency, because this value depends on the DOS and on the dc photon flux: the lower the DOS and the higher the dc flux, the higher the turn-on frequency. Then, in a second step, one can take the results at a "good" frequency and at different temperatures to get the DOS shape. As an illustration, the results obtained from Figs. 4(a) or 4(b) at $f = 3.5$ kHz (a frequency well above the turn-on frequen-

cy at F and $F/100$) where the temperature is varied from 150 to 450 K in 25-K steps are presented in Fig. 4(c). By this procedure the DOS we find is close to the original one but the characteristic temperature of the sharpest slope of the conduction-band tail is found equal to 300 K instead of the introduced 220 K for the reasons expressed above.

The features exposed in this section have been already identified on preliminary experimental results obtained on a -Si:H, which have been published elsewhere.²⁰

C. Influence of transport and trapping parameters

In this part the dc photon flux was fixed to $F/100$, in order to stay in regime (i) where the modulated photocurrent is not limited by recombination except close to the dark Fermi level at high temperatures. We have studied the influence of the transport and trapping parameters on the results of the MPC technique.

We have first checked the influence of the DOS itself. Indeed, the results of Sec. IV B show that, with the DOS introduced in the simulation (Fig. 1), and using the same values for the electron and hole mobilities and equal values for their attempt-to-escape frequencies, only part of the *electron* DOS can be probed. This is not linked to the type of the material (either N or P), but to the relative values of the electron DOS and of the hole DOS at $E_{\omega n}$ and $E_{\omega p}$, respectively. Indeed, if the DOS introduced in the calculations is reversed so that the electron DOS becomes larger than the hole DOS, then the DOS which is found using Eq. (29) corresponds to the *hole* trapping states, as shown in Fig. 5 (the mobilities of the carriers were both taken equal to $10 \text{ cm}^2\text{V}^{-1}\text{s}^{-1}$ and the attempt-to-escape frequencies were both taken equal to 10^{12} s^{-1} as in Figs. 3 and 4). In Fig. 5(a) the position of the dark Fermi level was maintained to its primitive value ($E_c - E_F = 0.75 \text{ eV}$) and the same artifact as observed in Fig. 4(a) around E_F is now observed around the symmetrical to E_F with respect to midgap. As already mentioned in Sec. II C, this is because the states lying deeper than 0.75 eV (either from E_c or E_v) always act as recombination centers, whatever the value of the dc generation rate. Figure 5(b) shows that shifting the Fermi level to midgap translates this artifact to deeper energies.

We have then studied the influence of the mobilities on the results of the MPC analysis with the standard DOS presented in Fig. 1 and with equal attempt-to-escape frequencies for both carriers ($\nu = 10^{12} \text{ s}^{-1}$). The hole mobility was increased to an unrealistic value for a -Si:H, $\mu_p = 100 \text{ cm}^2\text{V}^{-1}\text{s}^{-1}$, whereas the electron mobility was decreased to $\mu_n = 1 \text{ cm}^2\text{V}^{-1}\text{s}^{-1}$. In this case, the determination of the capture cross section σ was not accurate. Indeed, the contribution of the holes to the total dc current was always predominant ($\mu_p p_{\text{dc}} > \mu_n n_{\text{dc}}$), but the capture rate of the electrons was always greater than that of the holes ($c_n n_{\text{dc}} > c_p p_{\text{dc}}$). Thus, applying the procedure described in Sec. III can lead to errors of more than one order of magnitude for σ . Moreover, the σ values deduced this way depend on the dc photon flux, which could be interpreted as a dependence of σ upon energy. In Fig. 6(a), we present the DOS reconstructed by

means of Eqs. (29) and (30) using the hole parameters μ_p and ν_p which were supposed known. We observe that it is close to the *hole* DOS except in the range of energies R_1 indicated by two arrows. If we consider the slopes of the deduced DOS in the range R_1 it appears that the sharpest one is closer to the slope of the corresponding DOS on the conduction-band side. Since the attempt-to-escape frequencies were the same for holes and electrons the probed energies $E_{\omega n}$ and $E_{\omega p}$ were symmetrical with respect to midgap. The discrepancy observed in R_1 is explained by the fact that the ratio $N(E_{\omega p})/\mu_p$ in R_1 is higher than the ratio $N(E_{\omega n})/\mu_n$ in the range of energies symmetrical to R_1 with respect to midgap. This means that the majority carriers that contribute to the modulated photocurrent switch from holes to electrons when $N(E_{\omega p})/\mu_p$ becomes higher than $N(E_{\omega n})/\mu_n$. This is confirmed by the results presented in Fig. 6(b), where μ_n was further lowered by a factor of 10, $\mu_n = 0.1 \text{ cm}^2\text{V}^{-1}\text{s}^{-1}$, μ_p being kept equal to $100 \text{ cm}^2\text{V}^{-1}\text{s}^{-1}$, in order to have $N(E_{\omega p})/\mu_p$ always lower than $N(E_{\omega n})/\mu_n$. One can see that the problem observed in Fig. 6(a) in the energy range R_1 has completely disappeared, and that the DOS reconstruction is good, though the characteris-

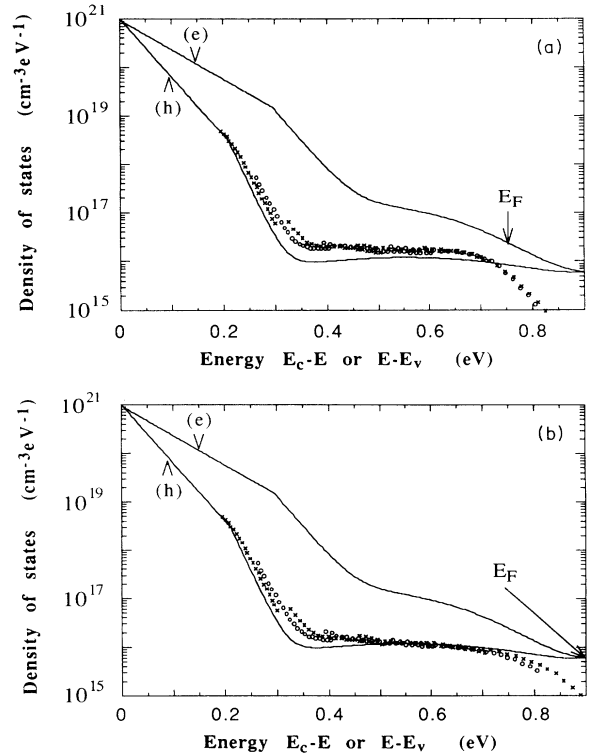


FIG. 5. Results of a simulation in which the introduced DOS is the symmetrical to that shown in Fig. 1 with respect to midgap. The DOS at the energy E_e on the conduction-band side, labeled by (e), is then always higher than the corresponding DOS at E_h such as $E_v - E_h = E_c - E_e$ on the valence-band side, labeled by (h). The DOS deduced from the MPC technique is the lower one. In (a), $E_c - E_F = 0.75 \text{ eV}$ results in a quenching of the measured DOS. This quenching disappears if E_F is at midgap as presented in (b).

tic temperature of the sharpest slope of the valence-band tail deduced from the results of the simulation is higher than the introduced one (about 500 K instead of 400 K) for the reasons explained in Sec. IV B. Note that the issue of whether electrons or holes give a major contribution to the dc photocurrent in *a*-Si:H is still a matter of research and was addressed recently by Yoon *et al.*²¹

With the DOS presented in Fig. 1, we have also studied the influence of the attempt-to-escape frequencies on the results of the MPC experiment. While the mobilities were taken equal to $\mu_p = \mu_n = 10 \text{ cm}^2\text{V}^{-1}\text{s}^{-1}$, the attempt-to-escape frequency for holes was decreased to $\nu_p = 10^{10} \text{ s}^{-1}$ whereas the attempt-to-escape frequency for electrons was maintained to its primitive value $\nu_n = 10^{12} \text{ s}^{-1}$. Again, this is a case where the experimental determination of a capture cross section would lead to significant errors, for the same reasons as in the case of very different mobilities ($\mu_p p_{\text{dc}} > \mu_n n_{\text{dc}}$ but $c_p p_{\text{dc}} < c_n n_{\text{dc}}$). The deduced DOS has been obtained by means of Eq. (29) taking into account the hole parameters

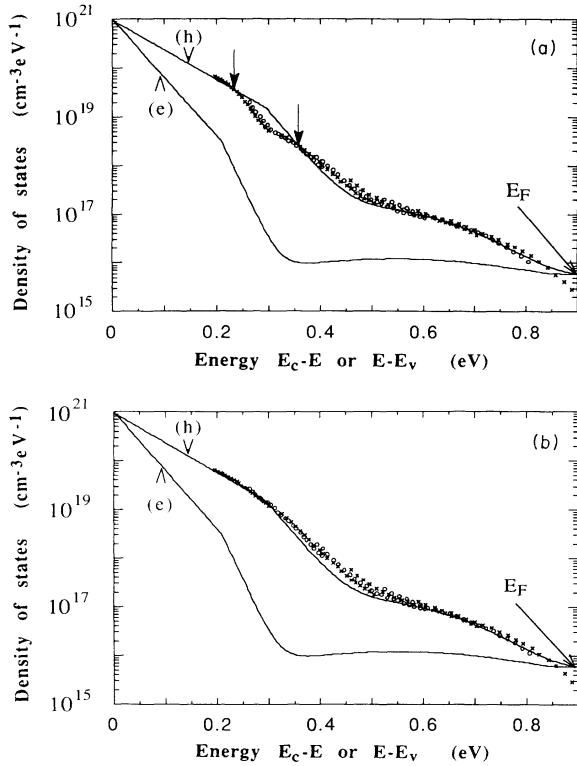


FIG. 6. Influence of the values of the free-carrier mobilities. The DOS of Fig. 1 has been introduced in the simulation. In (a) we have chosen $\mu_n = 1 \text{ cm}^2\text{V}^{-1}\text{s}^{-1}$ and $\mu_p = 100 \text{ cm}^2\text{V}^{-1}\text{s}^{-1}$, and the same attempt-to-escape frequencies ($\nu_n = \nu_p = 10^{12} \text{ s}^{-1}$). The DOS found from the MPC technique corresponds to the hole contribution except in the region indicated by the arrows, where the electronic contribution seems to be predominant. This transition from the hole to the electron predominant contribution disappears completely if the ratio between the mobilities is increased ($\mu_n = 0.1 \text{ cm}^2\text{V}^{-1}\text{s}^{-1}$, $\mu_p = 100 \text{ cm}^2\text{V}^{-1}\text{s}^{-1}$) as it is seen in (b).

and is presented in Fig. 7(a). Though the agreement between the introduced DOS and the deduced one seems rather good for high values of $E - E_v$, a discrepancy can be clearly seen for low values of $E - E_v$. It is observed in Fig. 7(a) and can be interpreted in the same way as the discrepancy observed in Fig. 6(a). In the ranges of frequencies and temperatures used to run the simulation the major contribution to the modulated photocurrent switches from one type of carrier to the other. The interpretation is complicated by the fact that the probed energies E_{on} and E_{op} are no longer symmetrical with respect to midgap since the attempt-to-escape frequencies depend on the type of carriers. Nevertheless, these attempt-to-escape frequencies are involved in logarithms in the energy scale [Eq. (30)], and therefore the symmetry has not completely disappeared. The switch from the hole to the electron predominant contribution occurs when the prod-

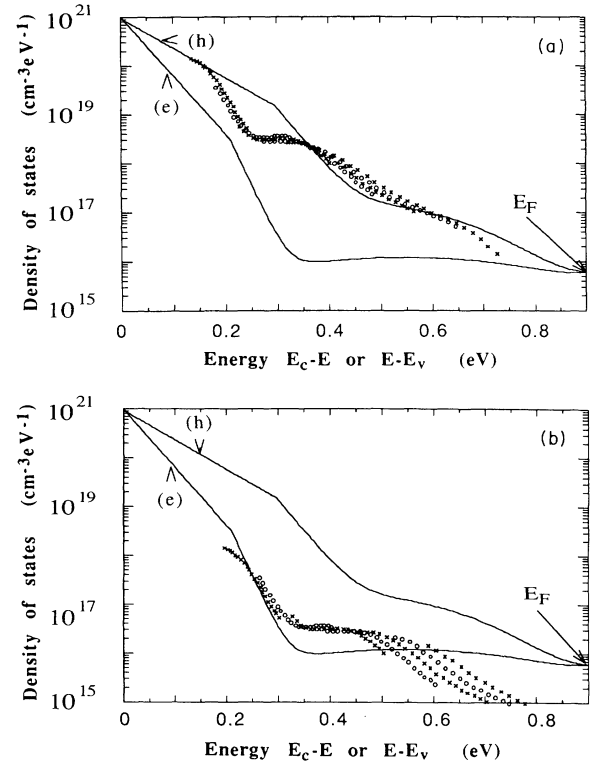


FIG. 7. Influence of the attempt-to-escape frequencies of the traps. The simulation was achieved with $\nu_n = 10^{12} \text{ s}^{-1}$ and $\nu_p = 10^{10} \text{ s}^{-1}$ and the same value of the mobilities for both carriers ($\mu_n = \mu_p = 10 \text{ cm}^2\text{V}^{-1}\text{s}^{-1}$). In (a) the DOS shape deduced from Eqs. (29) and (30) is obtained assuming that the hole contribution to the photocurrent is always predominant (using μ_p and ν_p instead of μ_p and ν_n). In (b) the results of the MPC simulation are plotted as if the electron contribution was always predominant. One can see that in neither case is a good agreement found between the introduced and the reconstructed DOS for the whole range of scanned energies. This comes from a transition of the major contribution to the modulated photocurrent from one type of carrier to the other that occurs when the temperature and the frequency, at which the MPC simulation is performed, are varied.

uct $N(E_{\omega_n})\nu_n$ is lower than the product $N(E_{\omega_p})\nu_p$. This is confirmed by Fig. 7(b) where the DOS shape is deduced using the electronic parameters. The agreement in the fit is reversed: the discrepancy occurs for high values of $E_c - E$ whereas the shape of the conduction-band tail is quite well reproduced. Note that this agreement occurs roughly in the energy range where the difference between the hole DOS and the electron DOS is the largest.

From the results presented in this section, we can see that in many cases, the simple treatment based on the phase shift and modulus of the modulated photocurrent can lead to a reliable DOS shape. To the question whether it is the electron or the hole DOS that is probed, we can answer that the trapping states explored by the MPC technique correspond to the type of carriers which exhibits the lower $\tilde{N}(E_\omega)\nu/\mu$ product. This point deserves more comments: in any amorphous semiconductor, there is always a competition between the transport of the carriers in the extended states and the trapping and release processes with the localized states. In the $\tilde{N}(E_\omega)\nu/\mu$ product, the transport is described by the mobility μ , whereas $\tilde{N}(E_\omega)\nu$ characterizes the trapping at E_ω . Taking into account the definition of ν [$\nu = \nu\sigma k_B TN(E_{BE})$, where $N(E_{BE})$ is the DOS at the corresponding band edge], the product $\tilde{N}(E_\omega)\nu$ can also be written as $\nu\sigma k_B TN(E_\omega)$, which is precisely the capture rate of the localized states contained in a $k_B T$ energy range around E_ω . From the very definition of E_ω , the emission rate of these states is simply equal to ω . The competition mentioned above is contained in the quantity:

$$\mu(\omega) = \frac{\mu\omega}{\nu\sigma k_B TN(E_\omega)}, \quad (35)$$

which represents the MPC sensitive trap-controlled mobility. Therefore, it is easily understood that, at a given ω , the modulated photocurrent will be controlled by the type of carriers which exhibits the higher $\mu(\omega)$, and consequently the lower value for $N(E_\omega)\nu\sigma/\mu$.

V. CONCLUSIONS

We have performed a theoretical analysis of the modulated photocurrent applied to amorphous semiconductors, taking into account the contributions of both types of carriers as it should be done for samples built in coplanar geometry and uniformly illuminated. Two main regimes have to be considered, depending on the measurement frequency, the temperature, and on the average light intensity. For a proper use of the MPC experiment, it is necessary to identify these two regimes, which are material dependent.

In the high-frequency regime, the modulated photocurrent is controlled by trapping and release processes. The frequency and temperature determine the energy position of the probed gap states relative to the nearest mobility edge. Since the two types of carriers contribute to the current, the deduced DOS can be representative either of the electron or of the hole trapping states. We

have shown that the probed states are those having the larger $\mu/\nu\sigma N$ ratio. This is simply interpreted in terms of a larger MPC sensitive mobility. A direct consequence is that, if the same type of carriers gives a predominant contribution to the ac photocurrent in the whole investigated frequency and temperature ranges, a frequency or temperature scan leads to a *relative* DOS spectroscopy by means of a simple treatment based on a unipolar assumption. On the contrary, we have shown by means of numerical calculations that, in the case of very different electron and hole DOS shapes combined with different mobilities or capture coefficients for electrons and holes, a transition from a major contribution of one type of carrier to the other type can occur in the ac photocurrent, even if the dc photocurrent is always dominated by the same type of carriers. The DOS deduced from the unipolar treatment can then be blurred.

In the low-frequency regime, the modulated photocurrent is controlled by recombination processes. Using the turn-on frequency corresponding to the transition between the two regimes, the *relative* DOS spectroscopy can be converted in *absolute* values, and the capture cross section for the dominant type of carriers can be deduced. Yet, the determination of a capture cross section is also subject to errors, if the major contributions to the dc current and to the total capture rate do not come from the same type of carriers.

As far as the *a*-Si:H is concerned, owing to the values of the mobilities, attempt-to-escape frequencies, and DOS suggested in the literature, the DOS probed by the MPC experiment performed on coplanar *a*-Si:H samples is very likely to be that of the *electron* trapping states. In any cases, sharp peaks or sharp variations of the probed DOS cannot be reconstructed precisely and care should be taken when deducing the band-tail slopes.

ACKNOWLEDGMENTS

Laboratoire de Génie Electrique de Paris is "Unité Associée au Centre National de la Recherche Scientifique No. D0127."

APPENDIX

1. Expressions of the coefficients of the system (13) of four equations

The coefficients of the system of four equations are the following:

$$A_n = c_n \int_{E_v}^{E_c} \left[1 - \frac{\bar{n}_{dc} + e_n(E)}{1/\tau(E) + \tau(E)\omega^2} \right] [1 - f_{dc}(E)] N(E) dE, \quad (A1)$$

$$A_p = c_p \int_{E_v}^{E_c} \left[\frac{\bar{n}_{dc} + e_n(E)}{1/\tau(E) + \tau(E)\omega^2} \right] f_{dc}(E) N(E) dE, \quad (A2)$$

$$B_n = c_n \omega \int_{E_v}^{E_c} \left[\frac{\bar{n}_{dc} + e_n(E)}{1/\tau^2(E) + \omega^2} \right] [1 - f_{dc}(E)] N(E) dE + \omega, \quad (A3)$$

$$B_p = c_p \omega \int_{E_v}^{E_c} \left[\frac{\bar{n}_{dc} + e_n(E)}{1/\tau^2(E) + \omega^2} \right] f_{dc}(E) N(E) dE, \quad (\text{A4})$$

$$A_n^* = c_n \int_{E_v}^{E_c} \left[\frac{\bar{p}_{dc} + e_p(E)}{1/\tau(E) + \tau(E)\omega^2} \right] [1 - f_{dc}(E)] N(E) dE, \quad (\text{A5})$$

$$A_p^* = c_p \int_{E_v}^{E_c} \left[1 - \frac{\bar{p}_{dc} + e_p(E)}{1/\tau(E) + \tau(E)\omega^2} \right] f_{dc}(E) N(E) dE, \quad (\text{A6})$$

$$B_n^* = c_n \omega \int_{E_v}^{E_c} \left[\frac{\bar{p}_{dc} + e_p(E)}{1/\tau^2(E) + \omega^2} \right] [1 - f_{dc}(E)] N(E) dE, \quad (\text{A7})$$

$$B_p^* = c_p \omega \int_{E_v}^{E_c} \left[\frac{\bar{p}_{dc} + e_p(E)}{1/\tau^2(E) + \omega^2} \right] f_{dc}(E) N(E) dE + \omega. \quad (\text{A8})$$

2. Evaluation of these coefficients

Simmons and Taylor¹² have shown that the occupation function $f_{dc}(E)$ can be expressed in the following way:

$$\begin{aligned} \text{if } E > E_F, \quad f_{dc}(E) \\ &= \frac{\bar{n}_{dc}}{\bar{n}_{dc} + \bar{p}_{dc}} \left[1 + \exp \left[\frac{E - E_{tn}}{k_B T} \right] \right]^{-1}; \end{aligned} \quad (\text{A9})$$

$$\begin{aligned} \text{if } E < E_F, \quad 1 - f_{dc}(E) \\ &= \frac{\bar{p}_{dc}}{\bar{n}_{dc} + \bar{p}_{dc}} \left[1 + \exp \left[\frac{E - E_{tp}}{k_B T} \right] \right]^{-1}; \end{aligned}$$

where E_F is the equilibrium Fermi level, \bar{n}_{dc} and \bar{p}_{dc} the capture rates of free electrons and free holes, respectively, E_{tn} and E_{tp} the quasi-Fermi-levels for trapped electron and trapped holes, respectively, defined by $e_n(E_{tn}) = e_p(E_{tp}) = \bar{n}_{dc} + \bar{p}_{dc}$. In the MPC experiment, the energy levels $E_{\omega n}$ and $E_{\omega p}$ such that $e_n(E_{\omega n}) = \omega$ and $e_p(E_{\omega p}) = \omega$ play an important role. When comparing $E_{\omega n}$ with E_{tn} , and $E_{\omega p}$ with E_{tp} , it can be seen that

- if $\omega \gg \bar{n}_{dc} + \bar{p}_{dc}$, then $E_{\omega n} > E_{tn}$ and $E_{\omega p} < E_{tp}$,
- if $\omega \ll \bar{n}_{dc} + \bar{p}_{dc}$, then $E_{\omega n} < E_{tn}$ and $E_{\omega p} > E_{tp}$,

Thus, two distinct cases have to be considered, whether ω is greater or smaller than $\bar{n}_{dc} + \bar{p}_{dc}$.

(a) Case (i): $\omega \gg \bar{n}_{dc} + \bar{p}_{dc}$. In the framework of a zero temperature approximation, where $f_{dc}(E)$ can be simplified in the following way:

$$\begin{aligned} \text{if } E > E_{tn}, \quad f_{dc}(E) &\approx 0; \\ \text{if } E_{tp} < E < E_{tn}, \quad f_{dc}(E) &\approx \frac{\bar{n}_{dc}}{\bar{n}_{dc} + \bar{p}_{dc}}; \\ \text{if } E < E_{tp}, \quad f_{dc}(E) &\approx 1; \end{aligned} \quad (\text{A10})$$

approximate expressions can be found for the weighting functions of the DOS in the integrals of Eqs. (A1)–(A8), and some of these coefficients are then found negligible compared with others. The dominant coefficients are A_n , B_n , A_p^* , and B_p^* , and their first-order approximate expressions are given by

$$A_n = c_n \frac{\bar{p}_{dc}}{\bar{n}_{dc} + \bar{p}_{dc}} \int_{E_{tp}}^{E_{tn}} N(E) dE + c_n \int_{E_{tn}}^{E_{\omega n}} N(E) dE, \quad (\text{A11})$$

$$B_n = \omega + c_n \int_{E_{tn}}^{E_c} G_n(E) dE, \quad (\text{A12})$$

$$A_p^* = c_p \frac{\bar{n}_{dc}}{\bar{n}_{dc} + \bar{p}_{dc}} \int_{E_{tp}}^{E_{tn}} N(E) dE + c_p \int_{E_{\omega p}}^{E_{tp}} N(E) dE, \quad (\text{A13})$$

$$B_p^* = \omega + c_p \int_{E_v}^{E_{tp}} G_p(E) N(E) dE, \quad (\text{A14})$$

where the weighting functions $G_n(E)$ and $G_p(E)$ can be written

$$G_n(E) = \frac{\omega e_n(E)}{e_n^2(E) + \omega^2}, \quad (\text{A15})$$

$$G_p(E) = \frac{\omega e_p(E)}{e_p^2(E) + \omega^2}. \quad (\text{A16})$$

The two functions $G_n(E)$ and $G_p(E)$ are sharp peaked functions centered, respectively, at $E_{\omega n}$ and $E_{\omega p}$, and they can be approximated by Dirac δ functions, so that

$$B_n = \omega + \frac{\pi}{2} c_n k_B T N(E_{\omega n}), \quad (\text{A17})$$

$$B_p^* = \omega + \frac{\pi}{2} c_p k_B T N(E_{\omega p}). \quad (\text{A18})$$

It is noteworthy that the function $G_n(E)$ is the same as the function $G_1(E)$ defined by Oheda³ [Eq. (11) in his paper], provided that E is above E_{Fn} (which is always verified since $\omega \gg \bar{n}_{dc} + \bar{p}_{dc}$). Moreover, in the framework of the statistics of Simmons and Taylor, the first term of Eq. (A11) can also be written as the reciprocal of the electron lifetime $1/\tau_n$. This shows that in our generalized treatment, the simplified expressions of A_n and B_n are in accordance with those of A and B defined by Oheda in his treatment of an unipolar electronic system. In our treatment, the electron lifetime τ_n appears naturally; moreover, we have also shown that the important level, as far as the electrons are concerned, is not the quasi-Fermi-level for *free* electrons E_{Fn} (as used by Oheda), but the quasi-Fermi-level for *trapped* electrons E_{tn} .

(b) Case (ii): $\omega \ll \bar{n}_{dc} + \bar{p}_{dc}$. Taking into account the definition of $\tau(E)$ [Eq. (11)], we can write: $\omega\tau(E) \ll 1$, whatever the value of the energy E in the band gap. If we neglect $\omega^2\tau^2(E)$ compared to 1, it is easily shown that $A_n = A_n^*$ and $A_p = A_p^*$. The system given by Eq. (13) can no longer be split into two subsystems holding, respectively, for the electrons and for the holes. However, this system can be solved analytically, and after quite cumbersome

some calculations, the following expressions are derived:

$$n_r = \frac{G_{ac}(B_p + B_p^*)\cos^2(\phi)}{A_n(B_p^* + B_p) + A_p(B_n^* + B_n)}, \quad (\text{A19})$$

$$n_i = \frac{G_{ac}(B_p^* + B_p)\sin^2(\phi)}{B_p B_n^* - B_n B_p^*}, \quad (\text{A20})$$

$$p_r = \frac{G_{ac}(B_n + B_n^*)\cos^2(\phi)}{A_n(B_p^* + B_p) + A_p(B_n^* + B_n)}, \quad (\text{A21})$$

$$p_i = \frac{G_{ac}(B_n^* + B_n)\sin^2(\phi)}{B_p B_n^* - B_n B_p^*}, \quad (\text{A22})$$

ϕ being given by

$$\tan(\phi) = \frac{B_p B_n^* - B_n B_p^*}{A_n(B_p^* + B_p) + A_p(B_n^* + B_n)}. \quad (\text{A23})$$

From the expressions (A19)–(A23) we then obtain

$$\frac{|I_{ac}|}{\cos(\phi)} = S q \xi G_{ac} \frac{\mu_n(B_p^* + B_p) + \mu_p(B_n^* + B_n)}{A_n(B_p^* + B_p) + A_p(B_n^* + B_n)}. \quad (\text{A24})$$

It can be easily shown from the expressions of A_n , A_p , B_n , B_n^* , B_p , and B_p^* , in which the approximation $\omega\tau \ll 1$ has been taken into account, that $\tan(\phi)$ varies as ω , whereas $|I_{ac}|/\cos(\phi)$ is independent of ω . In a first-order approximation, the coefficients are found to be determined by recombination, which means that the integrals describing these coefficients can be restricted to the domain between E_{rp} and E_{rn} and expressed in terms of the electron and hole lifetimes τ_n and τ_p defined by Taylor and Simmons.¹³ One then finally finds

$$\phi = 0 \quad (\text{A25})$$

and

$$|I_{ac}| = S q \xi G_{ac} (\mu_n \tau_n + \mu_p \tau_p). \quad (\text{A26})$$

- ¹C. Longeaud, G. Fournet, and R. Vanderhaghen, *Phys. Rev. B* **38**, 7493 (1988).
²G. F. Seynhaeve, R. P. Barclay, G. J. Adriaenssens, and J. M. Marshall, *Phys. Rev. B* **39**, 10196 (1989).
³H. Oheda, *J. Appl. Phys.* **52**, 6693 (1981).
⁴G. Aktas, C. Z. Çil, and E. Aktulga, *Appl. Phys. A* **48**, 237 (1989).
⁵R. Brüggemann, C. Main, J. Berkin, and S. Reynolds, *Philos. Mag. B* **62**, 29 (1990).
⁶G. Schumm, K. Nitsch, and G. H. Bauer, *Philos. Mag. B* **58**, 411 (1988).
⁷G. Schumm and G. H. Bauer, *Phys. Rev. B* **39**, 5311 (1989).
⁸H. Okushi, T. Takahama, Y. Tokomaru, S. Yamasaki, H. Oheda, and K. Tanaka, *Phys. Rev. B* **27**, 5184 (1983).
⁹H. Okushi, Y. Tokomaru, S. Yamasaki, H. Oheda, and K. Tanaka, *Phys. Rev. B* **25**, 4313 (1982).
¹⁰D. V. Lang, J. D. Cohen, J. P. Harbison, M. C. Chen, and A. M. Sergent, *J. Non-Cryst. Solids* **66**, 217 (1984).
¹¹W. Shockley and W. T. Read, *Phys. Rev.* **87**, 835 (1952).
¹²J. G. Simmons and G. W. Taylor, *Phys. Rev. B* **4**, 502 (1971).
¹³G. W. Taylor and J. G. Simmons, *J. Non-Cryst. Solids* **8-10**, 940 (1972).

- ¹⁴J. G. Simmons and G. W. Taylor, *J. Non-Cryst. Solids* **8-10**, 947 (1972).
¹⁵K. Hattori, Y. Niwano, H. Okamoto, and Y. Hamakawa, *J. Non-Cryst. Solids* **137&138**, 363 (1991).
¹⁶Note that one can also make use of the value I_{ac_0} of $|I_{ac}|$ at the plateau (for very low values of ω), since, from Eq. (25), the ratio I_{dc}/I_{ac_0} is simply equal to the ratio of the dc flux to the ac flux.
¹⁷R. Vanderhaghen and C. Longeaud, *J. Non-Cryst. Solids* **114**, 540 (1989).
¹⁸S. Aljishi, S. Jin, and L. Ley, in *Amorphous Silicon Technology*, edited by A. Madan, M. Thompson, P. C. Taylor, Y. Hamakawa, and P. G. Le Comber, MRS Symposia Proceedings No. 149 (Materials Research Society, Pittsburgh, 1989), p. 125.
¹⁹J. P. Kleider, D. Mencaraglia, and Z. Djebbour, *J. Non-Cryst. Solids* **114**, 432 (1989).
²⁰J. P. Kleider, C. Longeaud, and O. Glodt, *J. Non-Cryst. Solids* **137&138**, 447 (1991).
²¹H. Fritzsche, M. Q. Tran, B.-G. Yoon, and D.-Z. Chi, *J. Non-Cryst. Solids* **137&138**, 467 (1991).